An Efficient Snow Albedo Model for the Open and Sub-Canopy

RAE A. MELLOH[1], JANET P. HARDY[1], RONALD N. BAILEY[1], AND TOMMIE J. HALL[1]

ABSTRACT

A new model is presented for simulating snow surface albedo in the open and beneath a mixed-forest canopy. The model has modest input data requirements and is an efficient physically based parameterization that includes the dependency of albedo on solar zenith angle, cloud cover, canopy, snow grain size, litterfall, snowfall, snow depth, and partial snow cover. Measurements used in the model validation include incident spectral irradiances, wavelength-integrated visible and near-infrared albedos, snowfall records, snow depth, snow surface litter fractions, and quantity of fine litter in snow cores. Measured and modeled forest snow albedos were less than open snow albedos during the accumulation phase, when there was little or no surface litter. The model predicts lower albedos in the forest during the accumulation phase because of a spectral shift to less reflective wavelengths of incident radiation under the canopy. Snow grain size was important during both the accumulation and ablation phases. Surface litter fraction, incident spectra, snowpack depth, and partial snow cover were important factors lowering forest albedo during ablation. Despite lower mid-winter albedos in the forest, the snow melted more rapidly in the open. During late ablation, snow albedo in the open became lower than snow albedo in the forest, because of the thinner snow in the open. At the end of the ablation season, partial snow cover affected the albedo in the forest over a longer time period than in the open. Additional work is needed to improve the physical basis of the grain growth model used here and to develop a spatial albedo model for open and forested terrain.

Key words: snow, albedo, forest, litter, model

INTRODUCTION

Estimates of snow surface albedo for open fields and forests are sometimes desired at locations where solar radiation data are unavailable. Net solar radiation can be estimated from measurements of either incident or reflected solar radiation, or from modeled incident radiation if snow albedo is known. The albedo of optically thick snow in the open was modeled as a function of zenith angle and snow grain size by Marks (1988). The Marks model was based on Marshall and Warren's (1987) parameterization of the two-stream radiative transfer model of Wiscombe and Warren (1980) for the case of direct beam radiation. More recently, snow albedo was modeled with discrete ordinate radiative transfer methods; Glendinning and Morris (1999) used such a model to consider spectral and directional radiative transfer in snowpack temperature predictions. Hardy et al. (1998, 2000) presented a method to account for the effect of forest litter deposition rates within the multi-layered snowpack energy balance model, SNTHERM (Jordan 1991).

[1] U.S. Army Cold Regions Research and Engineering Laboratory, Engineer Research and Development Center, Hanover, New Hampshire

In this paper a relatively simple model is presented that extends the earlier model of Marks (1988) to estimate albedo in the open and an adjoining mixed forest, during the winter and the ablation season at a site in Vermont, USA. Melloh et al. (2001) previously documented the seasonal spectral albedo of the open and forested snowpacks at this site and concluded that the effect of litter on albedo was greatest during mid to late ablation when the snow was also becoming optically thin. In addition to solar zenith angle and snow grain size, the model allows consideration of the optical depth of snow, the ratio of incident visible and near-infrared (NIR) radiation for cloudy and clear conditions, the ratio of direct beam and diffuse radiation, differences in open and forest snow grain growth rates, the forest surface litter fraction, canopy modifications of incident irradiance spectra, and partial snow cover. The model inputs were kept at a minimum, requiring only latitude, longitude, timing of precipitation, temperature, snowdepth, and either the wet bulb temperature (or relative humidity) or the assumption of initial snow grain size for new snowfalls. The model was validated against open and mixed-forest albedo measurements.

SITE DESCRIPTION

The study sites include an open field at the Snow Research Station (SRS) of the Sleepers River Research Watershed (SRRW) near Danville, Vermont (44º29'28"N, 72º09'44"W), and a mixed-forest plot adjacent to the opening, both at 550-m elevation (Fig. 1). The dominant species of the mixed forest are balsam fir (*Abies balsamea*) and white birch (*Betula papyrifera*) at 52% and 43%, respectively. Melloh et al. (2001) provided additional details about the forest characteristics. The mean canopy openness calculated from hemispherical photographs, described later in this text, was 32%, and the average total transmittance (direct plus diffuse) was 42%. The climate at the site is one of cold winters and cool summers, with a mean annual temperature of 6ºC and mean temperature for December–February of –10ºC (Shanley et al. 1995). The mean annual precipitation is approximately 110 cm water equivalent, with 25% falling as snow. The maximum snow depth is typically around 1.0 m, and the maximum water equivalent accumulation of 0.23–0.30 m typically occurs in early March.

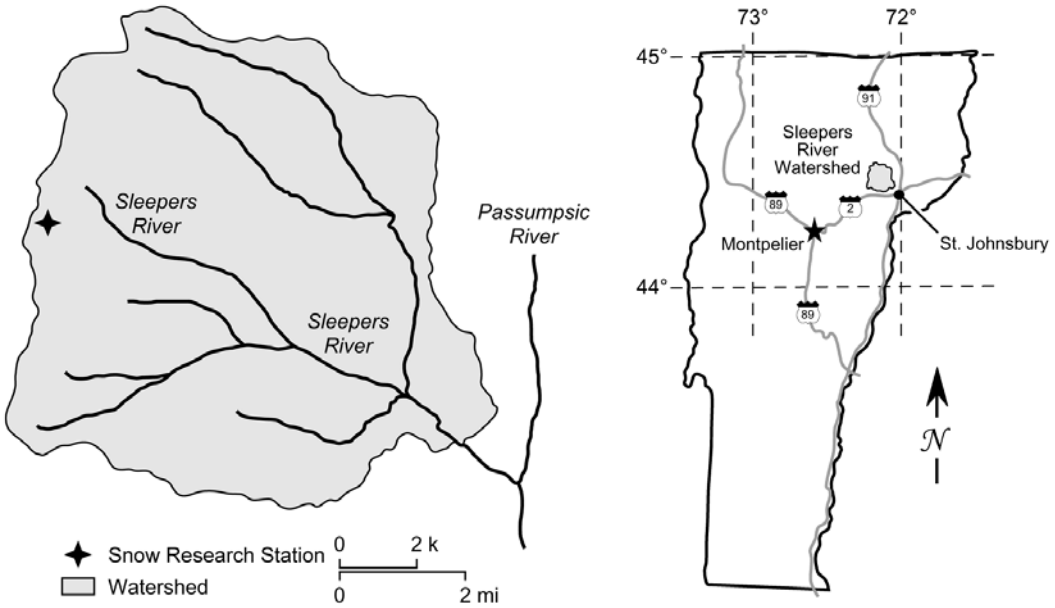

Figure 1. Location of the Snow Research Station in the Sleeper's River Research Watershed, Vermont, USA.

MEASUREMENTS AND OBSERVATIONS

Global Broadband Solar and Near-Infrared Radiation

Global shortwave radiation (285–2850 nm), both incident and reflected, was measured with a pair of pyranometers in the open and with an array of pyranometers in the forest using Eppley Laboratory, Inc. Precision Spectral Pyranometers. Incident and reflected NIR radiation (700–2850 nm) was also measured in the open. Canopy gaps in heterogeneous canopies make radiation sampling complex, requiring a number of pyranometers (Gay et al. 1971, Hendrie and Price 1978, Metcalfe and Buttle 1995, Ni et al. 1997). Incident and reflected radiation under the canopy was measured with a 20-radiometer array. Ten up-looking pyranometers were mounted on tripods 1.5 m above the forest floor, looking upward through the canopy. Ten down-looking pyranometers were suspended from tree mounts with inverted unipods that allowed height and level adjustment, and looked down at the snow surface. The heights of the down-looking pyranometers were adjusted through the season to between 0.5 and 0.75 m above the snow so that tree trunks were viewed at angles approaching the horizon, where the sensor's cosine response contributes little to the measurement. The distance of sensors from the nearest tree trunk was approximately 2.1 m. Radiation was measured every 10 seconds and time-averaged to 15-minute intervals. The data logger clocks were synchronized to the second and corrected weekly for time drift, which was minimal throughout the experiment. The incident and reflected radiation was calculated as the average of the ten sensors in each array, and albedos were calculated as the ratio of reflected to incident radiation for each 15-minute interval. Daily total albedos (Fig. 2) were calculated by summing the products of albedo and incident radiation for each interval through the day, and dividing by the sum of incident radiation for the day.

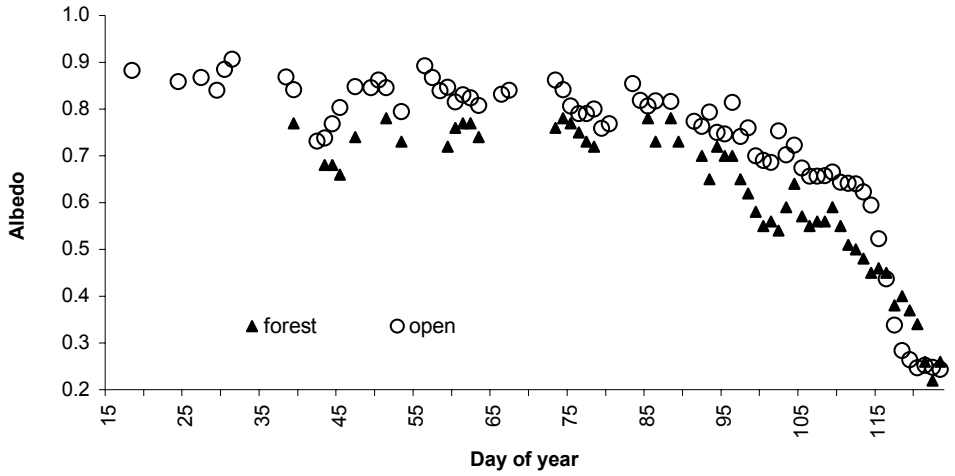

Figure 2. Total daily albedo in the forest and open, during the snow season of 2001.

Hemispherical photograph analyses of the canopy at the pyranometer locations were used to test whether or not the incident and reflected radiation arrays were similar enough in transmittance characteristics to compare, and to estimate the relative transmittance of direct and diffuse radiation components. The photographs (400 ASA black and white film) were taken at dusk with a Nikkor 8-mm hemispherical lens with a red filter, attached to a Nikon FM2 35-mm camera. Contrast between the canopy and the sky was enhanced by taking photographs when there was no direct sun in the canopy, and the red filter was used to improve contrast in overcast conditions (Pearcy 1991). The negatives were digitized with a Noritzu scanner to 1015 pixels across the diameter of the hemispheric image. Gap Light Analyzer software (Frazer et al. 1999) was used to calculate direct, diffuse, and total shortwave radiation transmittance through the canopy for incident and reflectance sensor sites. The software calculates the proportion of sunlight permitted through gaps

in the canopy at the sensor locations. The diffuse calculations assumed a Universal Overcast Sky (Hutchison et al. 1980), where regions of sky are assumed to be equally bright.

Spectral Measurements

Irradiance spectra that best represented open and forest settings for cloudy conditions during precipitation events, and clear to partly clear conditions between precipitation events, were chosen from a large number of spectral measurements made during the 2000 and 2001 snow seasons. The irradiance spectra selected for the open were taken during the 2000 snow season (Melloh et al. 2001), and those for the forest were taken during the 2001 snow season (Fig. 3). Spectra in the visible and NIR wavelengths (350–2200 nm) were measured with an Analytical Spectral Devices FieldSpec-FR using a full-sky remote cosine receptor having a 180º field of view (FOV). Individual spectral measurements consisted of averages of 100 samples in order to increase the signal-to-noise ratio. Representative spectral curves for open and forest were averages of 12 to 37 individual measurements taken over several minutes, or several tens of minutes (Fig. 3). The incident irradiance spectra collected under the canopy on a clear day sampled various degrees of shade and sun as the sensor was moved in a horizontal plane (Fig. 4). Spectra of the litter and wet ground beneath the snowpack, needed to correct albedo for optically thin and litter-contaminated snow, were available from the 2000 snowmelt season. Melloh et al. (2001) provides additional information on spectral measurement methods.

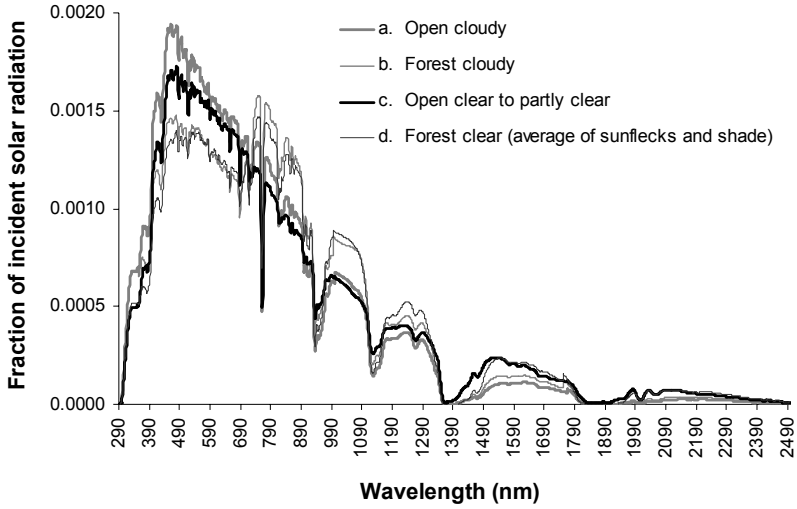

Figure 3. Fraction of incident solar radiation for each spectral wavelength during cloudy skies (open and forest), and during clear to partly clear skies (open and forest sun-shade). a.) 30 March 2000, the average of 37 measurements taken between 2:06 and 2:40 PM, b.) 9 April 2001, the average of 18 measurements taken between 1:53 and 2:11 PM, c.) 21 March 2000, the average of 12 measurements taken between 1:40 and 1:58 PM, and d.) 23 April 2001, the average of 15 measurements in sun and shade taken between 12:04 and 12:11 PM.

The FieldSpec-FR range (350–2500 nm) does not match the Eppley range (285–2850 nm) so adjustments were made to the spectral data to account for this difference. Incident irradiances in the 285- to 350-nm range were assumed to match the shape of a spectral irradiance curve for clear conditions available at http://www.cpc.ncep.noaa.gov. These corrected short wavelengths accounted for approximately 2.2% of the total incident irradiance. The full-sky remote cosine receptor is only responsive up to 2200 nm because of the properties of the white Delrin filter cap. Radiance spectra measured with a bare fiber optics cable (25º FOV) using techniques described by Melloh et al. (2001) were used to approximate irradiances from 2200 to 2500 nm. The radiance

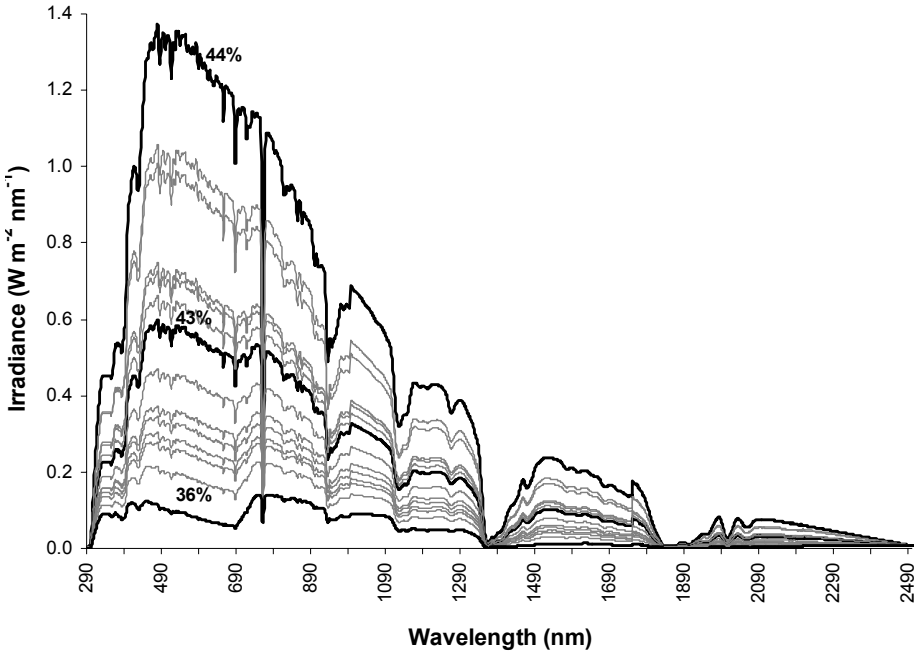

Figure 4. Irradiance spectra collected under a canopy on a clear day. The sensor was moved on a horizontal plane, to sample irradiance of sunny spots and various degrees of shade. The visible proportion of irradiance was 44% in the spot with the most sun, and 36% in the spot with the most shade. The spectra were taken on 28 April 2002 between 12:23 and 12:50 PM.

data were linearly increased to match the irradiance curves at 2200 nm. The corrected NIR data accounted for approximately 0.5% of the total incident radiation. Incident irradiance beyond 2500 nm was assumed to be negligible from inspection of published spectral irradiance curves (Kaufman 1989).

Meteorological and Snow Measurements

Meteorological data were collected at 2-m heights in the open (SRS) and in the adjacent forest (Table 1). The air temperature and relative humidity were measured with Rotronics MP-101A sensors. Precipitation was measured in the open as water equivalent, using a Belfort weighing-bucket gage. Campbell Scientific, Inc. SR50 sonic ranging sensors measured snow depth at single locations in the open and the forest. Spatially averaged snow depths were obtained on a near-weekly basis from 20 and 40 measurement points in the open and forest, respectively. Snowpack water equivalents (SWE) were measured on six dates between mid-February and the end of April. SWE data were the average of three collections with Adirondack samplers, at one location each in the open and the forest. A visual estimate of grain size was made in snow pits, and a photographic record was made of the surface and near-surface snow grains against an acrylic plate etched with a

Table 1. Sensor accuracy for meteorological variables measured.

Variables Measured	*Height (m)*	*Accuracy*	*Sensor*
Air temperature	2.0	± 0.2 °C	Rotronics MP101A
Relative humidity	2.0	± 1.5 %	Rotronics MP101A
Precipitation	2.0	5%	Belfort gage
Snow depth	2.0	± 0.01 m	Campbell Scientific SR50
Solar radiation	varied	± 4.2%	Eppley pyranometer

mm-grid scale. The density profile was sampled using a Taylor–LaChapelle 100-cm^3 density cutter, and the temperature of the snowpack was measured with dial stem thermometers. Oblique photographs taken of the snow surface under the down-looking radiometers on 19 and 28 April 2001 recorded dates of completely and partly snow covered conditions.

Large and Fine Litter Observations

Changes in surface litter were observed on a near-daily basis between 7 Feb and 30 April 2001 (DOY 38–120) at one location in the forest using a video camera system with a frame-grabber (640 × 480 pixel resolution) pointed perpendicularly to the snow surface. On 9, 13, 24, and 27 April 2001, point-in-time surveys of the littered snow surface in the forest were recorded on digital photographs using a Kodak DC5000 (1760 × 1168 pixel resolution) pointed perpendicularly to the snow surface at approximately 1-m height. Snow and litter fractions on each image were separated digitally by applying a threshold in Adobe Photoshop and finding the fraction of pixels the threshold level represented on the image histogram. The process was more precise on the digital photographs than on the video images. On the digital photographs twigs, leaves, needles, resin balls, and other small fragments were clearly resolved. Twigs, leaves, and needles were identifiable on the video images early in the snow season when the snow surface was nearer the camera, but late in the season as the snow surface dropped away from the camera, needles and other small fragments resulted in gray pixel areas that could be confused with less-reflective snow. The surface litter fractions determined with the four photographic surveys were used to guide the choice of threshold level for the video images.

Fine particle (2.5 μm to 2 mm) amounts in the snowpack at the time of maximum snow accumulation were sampled in 10 random snow tube cores (8 cm diameter) collected on 30 March 2001 in the open and in the forest by inserting an Adirondack sampler into the snow and transferring the snow into labeled white buckets. The Adirondack sampler and buckets were previously cleaned and rinsed with distilled water, and the Adirondack sampler was rinsed with distilled water after every five collections. The cleaning was done to exclude fine particles originating from sources other than the snowpack. The snow was allowed to melt in the hours prior to processing and the samples were filtered through a 2-mm sieve and then suctioned through pre-weighed 2.5-μm filters. The particles greater than 2 mm were not part of this analyses and were discarded.

MODEL DESCRIPTION

Two-Band Albedo Model

The albedo of optically thick snow in the open was modeled as a function of zenith angle and snow grain size using the method of Marks (1988), which was based on the parameterization of the Wiscombe and Warren (1980) model by Marshall and Warren (1987) for the case of direct beam radiation. The equations from Marks (1988) are:

$$\alpha_{v\theta} = [\alpha_{vmax} - a_{v0} r^{1/2}] + [a_{v\theta} r^{1/2}] [1 - \cos \theta] \quad (1)$$

and

$$\alpha_{nir\theta} = [\alpha_{nirmax} \exp(a_{nir0} r^{1/2})] + [(a_{nir\theta} r^{1/2}) + b_{nir\theta}] [1 - \cos\theta] \quad (2)$$

where the first term in each equation is for a hypothetical case of a solar zenith angle at nadir (θ = 0º) and the second terms are the adjustments for direct beam sun zenith angles other than 0º. During precipitation events the albedo was calculated using a fixed effective sun zenith angle of 50º for purely diffuse radiation (Warren 1982). Otherwise, mostly clear conditions were assumed and the albedo was taken as the weighted sum of 80% of the direct beam solution (Equations 1 and 2) and 20% diffuse radiation albedo. The maximum visible albedo α_{vmax} was taken as 1.0, and the maximum near-infrared albedo α_{nirmax} was taken as 0.85447 (Marks 1988), representing pure

snow conditions without contamination. The grain radius r (μm) is the radius of an ice sphere with optical properties equivalent to those of actual snow grains (Warren 1982). Actual snow grains are typically irregularly shaped or clustered (Colbeck 1986) and not easily related to optical grain size. Coefficients for the decay of albedo with grain size were derived from measurements in the Sierra Nevada, USA (Marks 1988) and are similar to those used by Marshall and Warren (1987). The decay coefficients for visible albedos ($a_{v,0}$ and $a_{v,\theta}$) were given as 2.0×10^{-3} and 1.375×10^{-3} $\mu m^{-½}$. The NIR coefficients (a_{nir0} and $a_{nir,\theta}$) were given as -2.123×10^{-2} and 2.0×10^{-3} $\mu m^{-½}$, with an offset coefficient ($b_{nir\theta} = 0.1$). The total albedo was then a weighted sum of visible and near-infrared fractions:

$$\alpha_\theta = \text{frac}_v \, \alpha_{v\theta} + \text{frac}_{nir} \, \alpha_{nir\theta} \; . \tag{3}$$

Visible fractions of 0.56 for cloudy conditions during precipitation events, and 0.50 for clear to partly clear conditions between precipitation events, were adopted for the open site, and match the proportions of visible wavelengths in the representative spectra measurements. In the forest, visible fractions adopted were 0.45 for cloudy conditions, and 0.43 for clear to partly clear conditions and also match the representative spectra measurements.

Grain Size and Growth

A model of grain growth was needed to calculate albedo over time. The Chebyshev polynomial (Acton, 1970) was adopted, after Marks (1988):

$$g = 1.0 - \{[(4 + 3t + t^2)/(2 + t + t^2)] - 1.0\} \tag{4}$$

where t is the time after a snowfall ends plus one day, and g is the percent of the grain growth range ($r_{max} - r_{min}$) achieved at that time. The new snow density (ρ_s g cm^{-3}) was computed as a function of the wet bulb temperature T_w (K) according to LaChapelle (1969):

$$\rho_s = 0.05 + 0.0017 \, (T_w - 258.16)^{1.5} \tag{5}$$

and the new grain size radius r_i (mm) was computed by the relationship

$$r_i = 0.08 + 55 \, \rho_s^4 \tag{6}$$

developed by Anderson (1976) at SRRW and converted to units of microns for use with Equations 1 and 2. The radius maximums chosen to obtain a reasonable fit with open albedos were 0.5 mm in mid-winter (days 18–40), 2.0 mm during a mixed-rain and snow period in February (days 40–50), 1.0 during early melt (days 50–100), and 2.8 during rapid melt and rainy weather (after day 100). During rain events, the prevailing grain size was retained instead of computing a new grain size. The snowpit observer recorded only slightly smaller grain sizes in the forest, and the forest grain growth range was set to 95% of that in the open to account for this difference.

Two-Stream Model Correction for Thin Snow and Surface Litter

Correction factors for visible (C_{vis}) and near-infrared (C_{nir}) were applied to the albedos calculated with Equations 1 and 2 for thin snow conditions. The correction factors were

$$C_{vis} = \alpha_{H,vis}/\alpha_{\infty,vis} \quad \text{and} \quad C_{nir} = \alpha_{H,nir}/\alpha_{\infty,nir} \tag{7}$$

where α_H is the albedo of a thin snowpack and α_∞ is the albedo of a snowpack of semi-infinite depth with the same density and grain size. Using the two-stream radiative transfer method of Choudhury and Chang (1979), as did Hardy et al. (1998), the visible and near-infrared albedos of the semi-infinite snowpack were computed at wavelength (λ in meters) increments of 5 nm in the 250- to 400-nm range and 10 nm in the 400- to 2850-nm range, as

$$\alpha_{\infty,\lambda} = 1 - [2(1 - \omega_\lambda)^{1/2} / ((1 - \omega_\lambda + 2\omega_\lambda \beta)^{1/2} + (1 - \omega_\lambda)^{1/2})] \quad (8)$$

where ω_λ is the single scattering albedo calculated by an approximation to Mie theory (Irvine and Pollack, 1968),

$$\omega_\lambda = (1/2) + (1/2) \exp(-1.67\, k_\lambda r) \quad (9)$$

where k_λ is the absorption coefficient for ice, and r is the grain radius in meters. The k_λ values used were those compiled by Warren (1984), updated by the values of Kou et al. (1993) in the 650- to 2500-nm range, and Perovich and Govoni (1991) in the 250- to 400-nm range. The two-stream solution for the thin snow case at each λ is

$$\alpha_{H,\lambda} = [(\alpha_{G,\lambda}\, \alpha_{\infty,\lambda} - 1)\, \alpha_{\infty,\lambda} + (\alpha_{\infty,\lambda} - \alpha_{G,\lambda})\, \exp^{-2A\tau})] / [(\alpha_{G,\lambda}\, \alpha_{\infty,\lambda} - 1) + \alpha_{\infty,\lambda}\, (\alpha_{\infty,\lambda} - \alpha_{G,\lambda}) \exp^{-2A\tau}] \quad (10)$$

where $\alpha_{G,\lambda}$ is the ground reflectance spectra and the exponent A is

$$A = (1 - \omega_\lambda)^{1/2}\, (1 - \omega_\lambda + 2\omega_\lambda \beta)^{1/2}\, \delta^{-1} \quad (11)$$

with modified Schuster-Schwartzschild parameters, ß and δ, taken as 0.065 and 0.57735, respectively. The optical thickness τ of the snow cover was calculated as

$$\tau = \gamma_e H \quad (12)$$

where H is the depth of the snowpack (m) and the extinction coefficient γ_e is

$$\gamma_e = (3/2r)(\rho / \rho_i) \quad (13)$$

where ρ is the bulk density of the snowpack, and ρ_i is the density of ice (0.916 g cm^{-3}). A snowpack density of 0.23 g cm^{-3} was used for the accumulation phase, in agreement with measured densities. A snowpack density of 0.35 g cm^{-3} was used for the ablation phase, chosen as representative of well-drained 0ºC snowpacks (McKay 1970) and is also in agreement with measured densities. The wavelength-integrated albedos for the visible and near-infrared bands were weighted by the fractional incident irradiances (f_λ):

$$\alpha_{\text{VIS or NIR}} = \sum (\alpha_\lambda f_\lambda) \quad (14)$$

summed over the 61 increments of visible wavelengths (350–700 nm) and the 230 increments of NIR wavelengths (700–3000 nm). The fractional incident irradiances (f_λ) in each wavelength increment were calculated from the measured incident irradiances representative of open and forest cloudy conditions (during precipitation events) and open and forest clear to partly clear conditions (between precipitation events). The spectral albedo computed by the two-stream radiative transfer model for pure snow was mixed with the spectral reflectance of litter (Melloh et al. 2001) using the surface litter fraction ($frac_L$) observations to obtain the litter-contaminated albedos (α_C) in the visible and NIR:

$$\alpha_{C\ \text{VIS or NIR}} = \text{frac}_L \sum (\alpha_{L,\lambda} f_\lambda) + (1 - \text{frac}_L) \sum (\alpha_\lambda f_\lambda)\ . \quad (15)$$

The snow cover beneath the down-looking sensors became incomplete and vegetation began to protrude above the snow between 19 and 28 April, and for that period of time the modeled albedos (Equation 15) were proportionately weighted with ground spectra albedos. The snow-covered area was calculated as the snow depth raised to the power of 0.125 in the forest and 0.05 in the open.

RESULTS

Radiation and Albedo Measurements in the Open and Forest

The hemispherical photograph analyses showed that the averaged transmittances for the sensor locations of the incident and reflected sensor arrays were nearly equal and could be expected to provide reasonable albedo estimates. The ratio of canopy transmittance for incident versus reflected measurement locations was 0.98 for total, 0.96 for direct beam, and 1.02 for diffuse radiation. The average transmittances of the direct and diffuse beam components of radiation at the incident measurement sites under the canopy were 42.8% and 41.4%, respectively, so it was not necessary to modify the forest diffuse–direct ratio from open conditions. Albedos in the forest were less than those in the open (Fig. 2) during the accumulation phase when the snow was optically thick. Partway through the ablation phase, the albedo in the forest began to exceed that of the more rapidly thinning snow in the open. The proportion of visible radiation measured with pyranometers in the open (Jan–May 2001) was 55% (45% NIR) during cloudy days with precipitation. The visible proportion for the periods between precipitation events increased mildly through the snow season. Computed as a cumulative average weighted by the strength of the incident radiation, the visible proportion was 48% for these clear to partly clear conditions.

Representative Spectra

Clouds absorb more of the NIR than visible wavelengths, and this was evident in the selected representative spectrum where there was a visible proportion of 50% for open-clear to partly clear, compared to 56% for open-cloudy conditions (Fig. 3). A mixture of clear to partly clear conditions was needed to represent the incident spectrum for periods of time between precipitation events. The spectrum selected were taken on a relatively clear winter day, with some NIR absorptance, probably due to high-altitude cirrus. The open-clear to partly clear visible component (50%) of the selected spectrum was close to the average visible proportion measured with pyranometers (48%) for time periods between precipitation events.

Sampling of variously shaded and bright sunflecks on the forest floor demonstrate a full distribution of spectral variation under the canopy on clear days (Fig. 4). The visible proportion ranged from 45% in bright spots to 36% in deeper shade for all measurements taken on this day, but it varied as low as 29% in spectra taken on other days. The representative spectrum was an average of fifteen measurements taken on 23 April 2001, and the visible proportion of the averaged spectra was 43%. Depletion of the visible wavelengths by absorption in the canopy was also seen in the cloudy day spectra, where the visible proportions averaged 45% (Fig. 3).

Litter

Estimates of the surface litter fraction showed almost no surface litter through the winter as the snowpack accumulated, then a dramatic increase during the ablation phase beginning around day 110 (Fig. 5). Mean weights of fine litter per volume of melted snow were 0.0166 g L^{-1} in the forest and 0.01 g L^{-1} in the open, with standard deviations of ± 65% and 50% of those respective means. The impact of fine litter on the albedo was considered to be within the error of the large litter fraction estimates and was not modeled separately.

Albedo

Modeled albedos compared well with the trend of albedo measurements in both the forest and the open throughout mid-winter and spring thaw (days 18 through 123). The model displayed responsiveness to grain growth and incident irradiance spectra in mid-winter (Fig. 6a and 7a) and the complexity of late spring's thinning snow, surface litter, and partial snow cover (Fig. 6b and 7b). The modeled albedo progressively decreased as model considerations were added for optical depth, canopy-modified incident spectra, litter, and snow-covered area. The influence of these modeled factors varied over the snow season. Table 2 compares the albedo results at noon. During the snow accumulation phase when the snow was deep and surface litter insignificant, modeled decreases in albedo (0.02 and 0.03 on days 29 and 78, respectively) were due to canopy modification

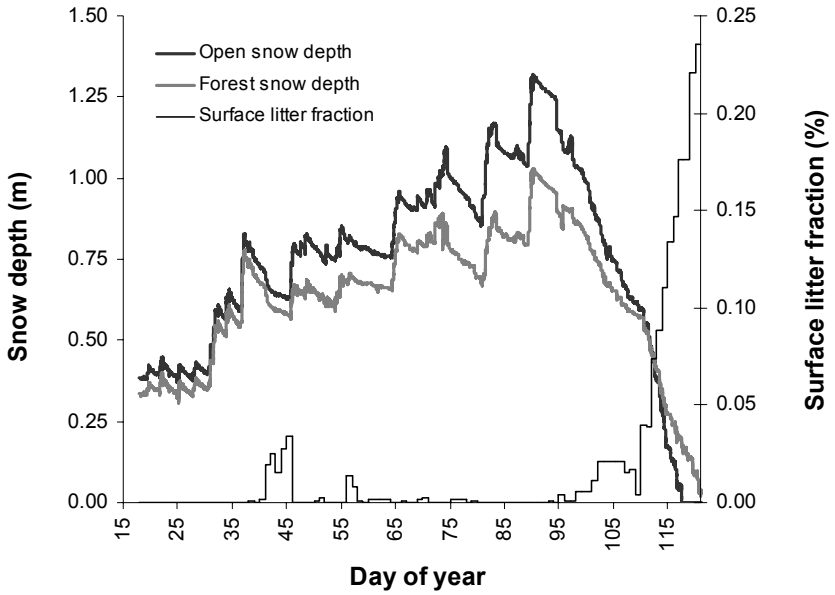

Figure 5. Snow depths in the open and forest, showing more rapid snow depletion in the open. Surface litter fractions, estimated from remote camera video and digital photographs, increase as the snowpack ablates.

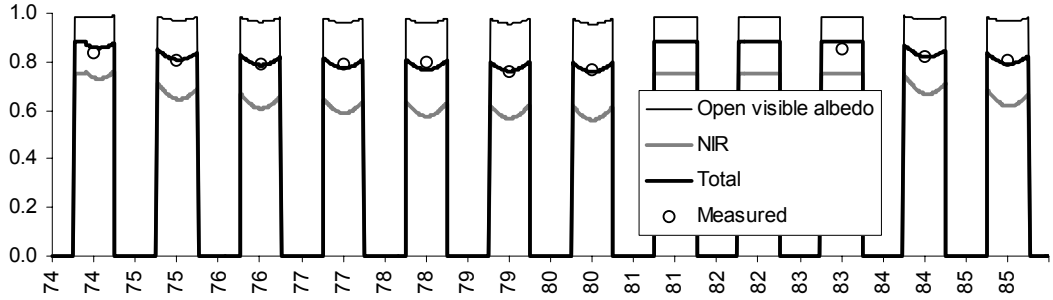

a. Open mid-winter.

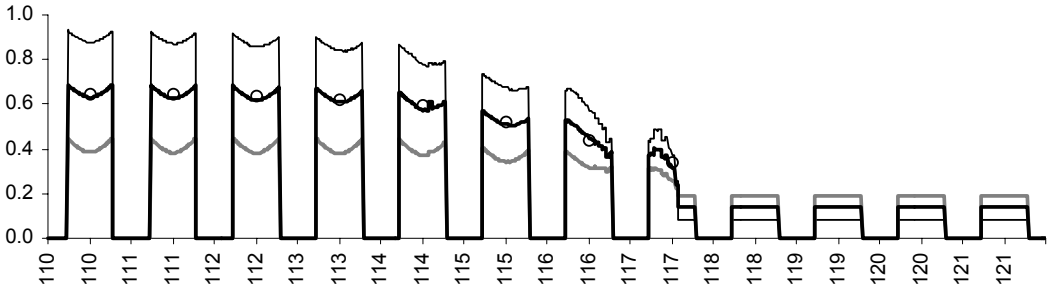

b. Open ablation.

Figure 6. Modeled total, visible and NIR albedos for mid-winter (a) and late spring (b) for the open site. Measured values are shown as total daily albedos. For a good match with calculated albedos, total daily albedos should be less than the observed morning and evening albedos but slightly higher than mid-day albedos.

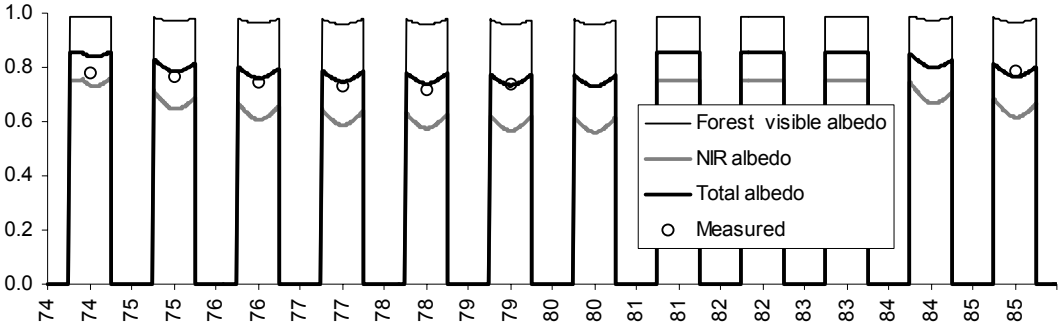

a. Forest mid-winter.

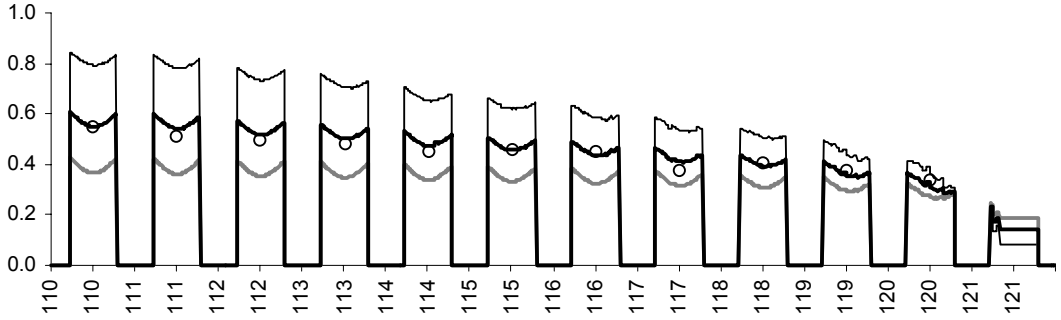

b. Forest ablation.

Figure 7. Modeled total, visible and NIR albedos for mid-winter (a) and late spring (b) for the forest site. Measured values are shown as total daily albedos.

Table 2. Influence of model considerations on computed albedo at noon.

Variable Added	*Day 29*	*Day 78*	*Day 114*	*Day 82*
	Clear to partly clear			Cloudy
Grain size	0.849	0.766	0.634	0.878
Optical depth in open	0.849	0.766	0.571	0.878
Optical depth in forest	0.849	0.766	0.597	0.878
Forest incident spectra	0.830	0.739	0.565	0.852
Litter	0.830	0.739	0.525	0.852
Partial snow cover	N/A	N/A	0.472	N/A
Direct/diffuse beam	0.828	0.740	0.475	0.858

of the incident spectra. During the ablation phase (day 114), there were decreases in albedo due to optical depth (0.06 and 0.04 for open and forest snow depths, respectively), canopy modification of incident spectra (0.03), presence of litter (0.04), and partial snow cover (0.05). Specifying diffuse and direct beam fractions had little impact on noon albedo, reducing it when the sun zenith angle was greater than 50º (day 29) and increasing it when the sun zenith angle was less than 50º (days 78, 82, and 114). The larger impact at noon was on overcast days (Table 2). The sun incidence angle effect was eliminated on overcast days (days 81–83, Fig. 6a and 7a) and reduced on clear to partly clear days.

DISCUSSION

Preferential absorption of radiation by the canopy resulted in a lower proportion of visible radiation incident to the snow surface in the forest, and because visible wavelengths are highly reflected by snow, this spectral shift to the NIR resulted in a lower albedo under the canopy. The decrease in visible transmittance observed here is analogous to Heute's (1987) canopy transmittance with varying levels of green cover. During mid-winter when the snow was fresh and essentially litter-free, the decrease in albedo due to modified incident spectra accounted for a part of the observed difference between the open and forest albedos (Fig. 2). The modeled forest albedos were slightly higher than measured albedos, and measurement error or choice of forest spectra might account for the discrepancy. Tree trunks and instrument shadows in the view of the sensor were minimized but not eliminated, and both lead to underestimates of measured albedo. The probability distribution for the visible fraction of incident irradiance under the canopy may not have been precisely defined by our averaged spectra measurements.

The simple albedo model presented here is applicable to other sites, provided site-specific adjustments are made. The incident spectra used here may not be directly transferable to other sites. Measurements specifically designed to represent the variation of incident spectra for open and forest and for time periods between and during precipitation events are needed as input to this model and, even for the present site, could be improved. In coniferous canopies that are more clumped and in discontinuous canopies, it may be critical to redefine the subcanopy spectra from what is used here. NIR broadband reflectance might be modified under some canopies, if more reflective NIR wavelengths within the NIR band are preferentially transmitted.

Future work needed includes improving the grain growth rate function used here to one that is more physically based rather than a simple function over time. A method based on air temperature and sun exposure would be useful for extending an albedo model to account for differences in grain size related to canopy openness, and terrain slope and aspect. Field studies of how snow grain properties in the forest vary from those in the open, and how sun exposure in canopy gaps and on sloping terrain influence grain growth, would be useful for validating a spatial albedo model. Snow grain properties as observed in snow pits are not easily related to optically equivalent grain sizes. Studies that link optical properties with seasonal snow grain classification schemes such as Colbeck's (1986) would be useful. Finally, while this albedo model will be useful in terms of the shortwave radiation balance beneath a forest canopy, a simple parameterized model of sub-canopy longwave (infrared) radiation would also be useful and would require consideration of the timing of heat storage and release by the canopy.

Glendinning and Morris (1999) noted that the Marks (1988) model gives a smooth diurnal albedo compared to the discrete ordinate solution. The model extensions presented here have not changed this characteristic substantially. Visible and NIR fractions, as well as direct beam and diffuse fractions, were available, and if these data had been used, an irregular pattern would have emerged. However, in the spirit of keeping data requirements at a minimum, our model assumes consistently cloudy conditions during precipitation events (100% diffuse) and clear to partly clear conditions otherwise (20% diffuse). In comparison with the SNTHERM litter model of Hardy et al. (1998), this simplified model does not explicitly track buried litter in subsurface layers that later re-emerge as the snowpack melts. Actual surface litter observations suggest that the surface litter fraction could be modeled at a modest accumulation rate between mid-winter precipitation events, reduced to 0% litter cover when new snow falls, and shifted to a high accumulation rate during melt to account for re-emerging litter. Some surface litter fraction rates of deposition for coniferous, deciduous, and mixed forests are suggested by Hardy et al. (1998, 2000) and Melloh et al. (2001).

CONCLUSION

This relatively simple model accurately explains measured albedo over a snow season in both forest and open environments, and the data requirements are modest. In the accumulation phase,

when snowpacks in the open and forest are similarly fresh and not littered, modeled and measured forest albedos were lower than the open, and this was attributed to alteration of the incident spectra by the forest canopy. Litter on the snow surface lowered forest albedo during the ablation phase. Despite the lower albedo in the forest, the snow melted more rapidly in the open. During late ablation, lower open than forest albedos were due to the differences in snow depth. Partial snow cover affected the albedo in the forest over a longer time period than in the open, where ablation was more rapid. A method to easily relate snow grains observed in the field with optical grain sizes used in modeling would improve model validation. A grain growth model sensitive to canopy openness and sun exposure is one approach to developing a spatial albedo model for open and forested terrain. Spectral irradiance curves representative of cloudy skies during periods of precipitation, and clear to partly clear skies between precipitation events are needed for application of this model to forest canopies that differ significantly from this site.

ACKNOWLEDGMENTS

This work was funded by Department of the Army project number AT24-SP-003, "Interaction of Solar Radiation, Litter and Albedo in the Forest During Snowmelt," Melloh R, Hardy J, and Robinson P. We would like to sincerely thank three anonymous reviewers for helpful comments that contributed to the completeness and clarity of this presentation.

REFERENCES

Acton FS. 1970. *Numerical Methods That Work*. Harper and Row: New York; 541 pp.

Anderson EA. 1976. A point energy and mass balance model of a snow cover. Silver Spring, MD: U.S. National Oceanic and Atmospheric Administration, *NWS Technical Memorandum HYDRO-17*.

Colbeck SC. 1986. Classification of seasonal snow cover crystals. *Water Resources Research* **22**: 59S–70S.

Choudhury BJ, Chang ATC. 1979. Two-stream theory of reflectance of snow. *IEEE Transactions of Geoscience and Electronics* **17**: 63–68.

Frazer GW, Canham CD, Lertzman KP. 1999. *Gap Light Analyzer (GLA), Version 2.0: Imaging software to extract canopy structure and gap light transmission indices from true-color fisheye photographs, Users manual and program documentation.* Simon Fraser University, Burnaby, British Columbia, and the Institute of Ecosystem Studies, Millbrook, New York; 36 pp.

Gay LW, Knoerr KR, Bratten MO. 1971. Solar radiation variability on pine plantation floor. *Agricultural Meteorology* **8**: 39–50.

Glendinning JHG, Morris EM. 1999. Incorporation of spectral and directional radiative transfer in a snow model. *Hydrological Processes* **13**: 1761–1772.

Hardy JP, Davis RE, Jordan R, Ni W, Woodcock CE. 1998. Snow ablation modeling in a mature aspen stand of the boreal forest. *Hydrological Processes* **12**: 1763–1778.

Hardy JP, Melloh RA, Robinson PB, Jordan R. 2000. Incorporating effects of forest litter in a snow process model. *Hydrological Processes* **14**: 3227–3237.

Hendrie LK, Price AG. 1978. Energy balance and snowmelt in a deciduous forest. In *Proceedings, Modeling of Snow Cover Runoff*, Colbeck, S.C. and M. Ray (editors), U.S. Army Cold Regions Research and Engineering Laboratory: Hanover, New Hampshire.

Huete AR. 1987. Soil-dependent spectral response in a developing plant canopy. *Agronomy Journal* **79**: 61–68.

Hutchison BA, Matt DR, McMillen RT. 1980. Effects of sky brightness distribution upon penetration of diffuse radiation through canopy gaps in a deciduous forest. *Agriculture and Forest Meteorology* **22**: 137-147.

Irvine WM, Pollack JB. 1968. Infrared optical properties of water and ice spheres. *Icarus* **8**: 324–360.

Jordan R. 1991. *A one-dimensional temperature model for a snow cover: Technical documentation for SNTHERM.89*. Special Report 91-16. U.S. Army Corps of Engineers, Cold Regions Research and Engineering Laboratory: Hanover, New Hampshire.

Kaufman YJ. 1989. The atmospheric effect on remote sensing and its correction. In Asrar G. (ed.), *Theory and Applications of Optical Remote Sensing,* John Wiley and Sons: New York; 734 pp.

Kou L, Labrie D, Chylek P. 1993. Refractive indices of water and ice in the 0.65- to 2.5-micron spectral range. *Applied Optics* **32**: 3531–3540.

LaChapelle ER. 1969. *Properties of snow*, prepared for Hydrologic Systems course presented by College of Forest Resources, Nov. 17–18. University of Washington: Seattle; 21 pp.

Marks, D. 1988. Climate, energy exchange, and snow melt in Emerald Lake watershed, Sierra Nevada. PhD Dissertation, Departments of Geography and Mechanical Engineering, University of California at Santa Barbara.

Marshall SE, Warren SG. 1987. Parameterization of snow albedo for climate models. In Goodison BE and Barry RG (ed.), *Large Scale Effects of Seasonal Snow Cover*, IAHS-AIHS Publication No.166. International Association of Hydrological Sciences: Wallingford, UK, pp. 43–50.

McKay GA. 1970. *Precipitation*. In Gray DM (ed.), *Handbook on the Principles of Hydrology*. Port Washington, New York: Water Information Center, Inc.

Melloh RA, Hardy JP, Davis RE, Robinson PB. 2001. Spectral albedo/reflectance of littered forest snow during the melt season. *Hydrological Processes* **15**: 3409–3422.

Metcalfe RA, Buttle J. 1995. Controls of canopy structure on snowmelt rates in the boreal forest. In *Proceedings Eastern Snow Conference*, 249–258.

Ni, W, Li X, and Woodcock CE. 1997. Transmission of solar radiation in boreal conifer forests: Measurements and models. *Journal of Geophysical Research* **102**: D24: 29,555–29,566.

Pearcy RW. 1991. Chapter 6, Radiation and Light Measurements. In Pearcy RW, Ehleringer J, Mooney HA, Rindel PW (ed.), *Plant Physiological Ecology, Field Methods and Instrumentation*. Editors: Pearcy RW, J Ehleringer J, Mooney HA, Rundel PW, Chapman and Hall, New York.

Perovich DK, Govoni JW. 1991. Absorption coefficients of ice from 250 to 400 nm. *Geophysical Research Letters* **18**(7): 1233–1235.

Shanley JB, Sundquist ET, Kendall C. 1995. *Water, energy, and biogeochemical budget research at Sleeper's River Research Watershed, Vermont.* U.S. Geological Survey, Open-File Report 94; 475 pp.

Warren SG. 1982. Optical properties of snow. *Review of Geophysics and Space Physics* **20**(1): 67–89.

Warren SG. 1984. Optical constants of ice from the ultraviolet to the microwave. *Applied Optics* **23**: 1206–1225

Wiscombe WJ, Warren SG. 1980. A model for the spectral albedo of snow, I. Pure snow. *Journal of Atmospheric Science* **37**(12): 2712–2733.